Wang, Z.; Huang, Y.; Srinivasan, A.; Zheng, L.; Beckmann, F.;
Kainer, K.U.; Hort, N.:

Hot tearing susceptibility of binary Mg–Y alloy castings

In: Materials and Design (2012) Elsevier

DOI: 10.1016/j.matdes.2012.12.044

Hot tearing susceptibility of binary Mg-Y alloy castings

Zhi Wang[1,2,*], Yuanding Huang[1], Amirthalingam Srinivasan[1], Zheng Liu[2], Felix Beckmann[1], Karl Ulrich Kainer[1], Norbert Hort[1]

1 Institute of Materials Research, Helmholtz-Zentrum Geesthacht, Max-Planck-Str. 1, 21502 Geesthacht, Germany
2 School of Materials Science and Engineering, Shenyang University of Technology, Shenyang 110870, China

Abstract:

The influence of Y content on the hot tearing susceptibility (HTS) of binary Mg-Y alloys has been predicted using thermodynamic calculations based on Clyne and Davies model. The calculated results are compared with experimental results determined using a constrained rod casting (CRC) apparatus with a load cell and data acquisition system. Both thermodynamic calculations and experimental measurements indicate that the hot tearing susceptibility as a function of Y content follows the "λ" shape. The experimental results show that HTS first increases with increase in Y content, reaches the maximum at about 0.9 wt.% Y and then decreases with further increase the Y content. The maximum susceptibility observed in Mg-0.9 wt.% Y alloy is attributed to its coarsened columnar microstructure, large solidification range and small amount of eutectic at the time of hot tearing. The initiation of hot cracks is monitored during CRC experiments. It corresponds to a drop in load increment on the force curves. The critical solid fractions at which the hot cracks are initiated are in the range from 0.9 to 0.99. It is also found that it decreases with increasing the content of Y. The hot cracks propagate along the dendritic or grain boundaries through the interdendritic separation or tearing of interconnected dendrites. Some of the formed cracks are possible to be healed by the subsequent refilling of the remained liquids.

Keywords: Mg alloy; Hot tearing; Thermodynamic; X-ray micro-tomography; Grain structure

*Corresponding author:

Email: zhi.wang@hzg.de

Tel.: +49 (0) 4152 87 1966

Fax: +49 (0) 4152 87 1909

1. Introduction

Hot tearing (or hot cracking) is known as one of the most fatal solidification defects commonly encountered during casting. Previous studies have revealed that this phenomenon occurs in the mushy zone of a freezing alloy and the solid phase of casting is formed by a continuous network of grains. Although it has been investigated for decades, the understanding still stands at a qualitative stage [1-2]. The factors dominating the formation and susceptibility of hot tears include alloying elements, freezing range, amount of eutectic phases and solidification rate [3]. So far, the investigations on hot tearing are mainly focused on the steels and aluminium alloys [4-5]. A comprehensive review on hot cracking of aluminum alloys has been published by Eskin et al. [2]. In contrast, only few works have been reported on the hot tearing of Mg alloys.

Investigations on the castability of Mg alloys indicated that castings are often prone to hot tearing defects. The selected alloys for the investigations of hot tearing are mainly Mg-Al series [6-11]. Wang et al. [12] used a quantifying method to monitor the temperature at which the hot tearing occurs. They concluded that the occurrence of eutectic induces the hot tearing of AZ91 alloy. After the addition of rare earths (cerium-rich mischmetal) to AZ91 alloy, the hot tearing susceptibility reduces [13]. Cao et al. [6-7] also surveyed the effects of alloying elements such as Ca and Sr on the hot tearing susceptibility of Mg-Al alloys. Their results demonstrated that these two alloying elements improve the castability and decrease the hot tearing susceptibility of Mg-Al alloys. Recently, Zhou et al. [14-15] used thermodynamic calculations and a quantitative method to evaluate the hot tearing of binary Mg-Zn alloys, which are the base alloys to be used for the development of wrought Mg alloys such as Mg-Zn-RE (rare earths). They found that the hot tearing of these alloys is largely influenced by both the content of Zn and mold temperature. The influence of Zn content on the hot tearing susceptibility follows the "λ" shape. It is also found that the addition of Y to Mg-Zn alloys alleviate the hot tearing [16]. The beneficial effects are attributed to the facts that Y addition increases the solidus temperature, shorten the terminal solidification path and reduce the terminal freezing range. Besides the investigations on the influences of respective chemical compositions on HTS, the effects of casting conditions such as the effect of

cooling rate on HTS were also sometimes explored in these above mentioned works such as the effect of cooling rate [14-15].

Considering the fact that the Y element plays a very important role in modifying the properties of Mg alloys [17-19], the investigations on the effects of Y on HTS of Mg alloys should be very interesting. The addition of Y not only improves the mechanical properties but also increases the corrosion resistance [20]. Mg-Zn-Y alloys have recently been reckoned as one of the most promising wrought Mg alloys for practical applications. However, the effects of Y on the castability of Mg alloys such as hot tearing is not yet well understood. The related mechanisms of hot tearing in Mg alloys containing Y still remain somewhat unclear. Therefore, the present work investigates the hot tearing susceptibility of binary Mg-Y alloys, and the influences of Y content on HTS of Mg alloy will be discussed.

2. Prediction of crack susceptibility coefficient based on Clyne and Davies model

The hot tearing criterion proposed by Clyne and Davies is based on the assumption that the liquid feeding can not accommodation the strains developed during solidification [21-22]. The last stage of freezing is considered as a critical stage to hot tearing. In their model, a cracking susceptibility coefficient (CSC) was proposed, which is defined by the ratio of t_V, the vulnerable time period where the hot tearing may develop, and t_R, the time available for the stress relief process where both the mass feeding and liquid feeding occur (Fig.1). The CSC reads:

$$CSC = \frac{t_V}{t_R} = \frac{t_{0.99} - t_{0.9}}{t_{0.9} - t_{0.4}} \tag{1}$$

Where $t_{0.99}$ is the time when the volume fraction of solid, f_S is 0.99, $t_{0.9}$ is the time when f_S is 0.9 and $t_{0.4}$ is the time when f_S is 0.4. The larger CSC value means the higher tendency of hot tearing.

As shown in the above equation (1) and Fig.1**,** in order to calculate the CSC, the variant fractional time at a specified solid fraction or liquid fraction should be known. This can be done by the following steps:

1) With using Scheil's modeling, the volume fraction of solid phase as a function of temperature is first calculated using thermodynamic software Pandat and PanMg 8.0 thermodynamic database. In Clyne and Davies model, the Scheil's assumption was considered to be reasonable for the solidification conditions encountered during castings.
2) The second step is the determination of temperature profile as a function of time, i.e. the cooling curve.

In order to predict the variation of the cracking susceptibility coefficient with alloy composition, it is necessary to design a series of alloys with different Y contents. The range of Y content considered is from 0.2 to 8.0 wt.% which is less than its maximum solubility in Mg at the eutectic temperature [23-24]. The volume fraction of solid phase as a function of temperature is shown in Fig.2. The content of Y has a large influence on the freezing range and the melting point. Above 610 to 640 °C the solid fraction reduces quickly, and below 610 to 640 °C it changes slowly. The specified temperature above which the solid fraction changes quickly closely depends on the content of Y. The melting points of Mg-Y alloys change from 650 to 632 °C when the content of Y increases from 0.2 to 8.0 wt.%.

In Clyne and Davies investigations, for calculating cooling curve, constant partition coefficient and liquidus slope were used [21-22]. Also it was assumed that both the liquidus and solidus were approximately linear. Actually, this may not be true. The liquidus and solidus lines in the phase diagram are not linear. In order to improve the accuracy of calculated results, in the present calculation the partition coefficient and liquidus slope were calculated using PanEngine module in Pandat software based on thermodynamic database PanMg 8.0. PanEngine is a collection of C++ classes, which performs some related thermodynamic and equilibrium calculations [25]. The calculated partition coefficient and liquidus slope of the Mg-Y alloy is shown in Fig.3, which clearly

indicates that both the partition coefficient k and liquidus slope m_L vary with temperatures. The value of the partition coefficient increases from 0.19 to 0.27 as the temperature decreases from 650 to 632 °C. The liquidus slope also changes from 6.8 to 8.5 in the temperature range from 650 to 632 °C.

The cooling curves could be estimated using three different modes: mode 1 with a constant cooling rate, $dT/dt = \text{constant}$; mode 2 with a constant heat flow, $dQ/dt = \text{constant}$ and mode 3 with a heat flow proportional to the square root of time, $dQ/dt \propto t^{-1/2}$ [21]. The typical calculated cooling curves for Mg-1.5 wt.% Y alloy under these three cooling conditions are shown in Fig.4. After comparing the experimental results, the calculated results using the mode 3 are found close to the realistic situation. Thus, all CSC values are calculated using the mode 3 cooling condition in the present investigation. Fig.5 shows the calculated CSC value as a function of the content of Y for the binary Mg-Y alloys. The curve follows the typical "λ" shape. The hot tearing susceptibility first increases with the content of Y, reaches a maximum at 1~2 wt.% Y and then decreases with further increasing the content of Y.

3. Experiments

3.1 Melting

Binary Mg alloys containing 0.2, 0.9, 1.5 and 4 wt.% Y were prepared for the present study. 350 g of Mg was molten in a mild steel crucible under a protective gas mixture of high pure Ar+0.2% SF_6. Pure Y was added to the melt at 700 °C. After stirring the molten alloys at 80 rpm for 2 min. and keeping for 5 min. at pouring temperature 750 °C, the molten alloys were cast into a constraint rod casting (CRC) mold, which was coated with a thin layer of boron nitride. The mold was preheated to a temperature (T_{mold}) of 250 °C. The castings were extracted from the mold after solidification and then examined for cracks. Each test was repeated for 3 times.

3.2 Hot tearing tests

The previously developed setups include ring type testing, cold finger testing, backbone mold testing and constrained rod testing, and so on [6, 16, 26-27], normally measure the hot tearing susceptibility in a qualitative way. In order to assess the hot tearing susceptibility quantitatively, a hot tearing setup based on the previously developed constrained rod testing was developed (Fig.6). Different from the previous setups, a load cell was attached in the present setup so that the evolution of contraction force during solidification can be recorded, which is quite an important information to show when the hot tearing initiates and how it propagates. All these information is very important to understand the mechanism of hot tearing.

The developed system consisted of a constrained rod casting (CRC) mold, a contraction force measurement system with a load cell, a data logging unit and a data recording program. The hot tears always occurred at the junction of the sprue and the horizontal bar. The mold consisted of two parts: vertical sprue and horizontal circular rod with a length of 148 mm. The sprue was open to the air at the top and connected to the rod portion of the mold near the bottom. The diameter of the rod portion of the mold was 12.5 mm at sprue end and 10 mm at the opposite end. This slight taper was provided to reduce friction between the mold and casting. At the opposite end of the sprue, a 53 mm long steel stud with a diameter of 6 mm was inserted into the rod portion of the mold and connected to a load cell (max. 2 kN) as illustrated (Fig.6). This steel stud provided a partial constraint to the movement of casting in the mold during solidification. The developed force was measured by the load cell. The force, mold temperatures at different positions and temperature of the solidifying casting at the hot spot area were recorded. The force curve (force vs. time) and cooling curve (temperature vs. time) were used for analyzing the hot tearing.

3.3 Microstructure analysis

The grain morphology and cracks were investigated on the cross section of the rod near the sprue-rod junction. In order to understand the crack propagation, the microstructures on the longitudinal cross section of the rod at the sprue-rod junction were also observed.

After polished the samples were chemically etched in a solution of 8 g picric acid, 5 ml acetic acid, 10 ml distilled water and 100 ml ethanol. They were observed using Reichert-Jung MeF3 optical microscope. A Zeiss Ultra 55 (Carl Zeiss GmbH, Oberkochen, Germany) Scanning Electron Microscope (SEM) equipped with Electron Dispersive Spectrometer (EDS) was used to study the fracture surfaces and also the crack propagations.

3.4 Hot tearing volume measurement

The hot tearing susceptibility was usually evaluated by the length and width of open cracks observed on the surfaces of rods [6, 16]. The shortness of this method is that the closed cracks inside the rods cannot be counted. Thus, the measured values are not so accurate. In the present paper, the hot tearing susceptibility is characterized by measuring the volume of cracks using 3D X-ray tomography, which can detect not only the surface cracks but also the inside cracks. The results obtained by this method are much more believable compared with the previous methods.

X-ray micro-tomography is a non-destructive, three-dimensional characterization method that has been applied to a number of fields within materials science [28-29]. The technique allows imaging the internal microstructural features by measuring variations in intensity of a transmitted X-ray beam through a rotating specimen. In the present study, the hot tearing susceptibility was evaluated using X-ray tomography in an X-ray tube-based high resolution tomography (*nanotom*® *s* - phoenix, GE Measurement & Control Solutions, Germany). The 3D volume reconstruction was made from the 2D projections (with a filtered back projection algorithm) using *datos|x2.0 reconstruction* software (phoenix, GE Measurement & Control Solutions, Germany). The resolution achieved after reconstruction of the volume in the region of interest was of about 20 μm. Further data processing, including normalization and alignment of the 3D-data sets, the segmentation and characterization of the crack volume was applied using the software IDL 8.1 (Exelis Visual Information Solutions, Inc.). Cylindrical samples of diameter approximately 12.5 mm machined from the CRC mould castings, as shown in Fig.7, were

used for the tomography measurements. The average crack volume of minimum two samples for each alloy measured is considered.

4. Results

4.1 Hot tearing curves

Fig.8 shows the experimental hot tearing curves of Mg-Y alloys with different contents of Y. The detailed characterization of hot tearing curves, including the definition of hot tearing initiation temperature (T_i) and crack propagation can be found elsewhere [14-15]. On all hot tearing curves, a slight reduction in the load was observed at the beginning of pouring. This is possibly due to the molten melt pressure exerted on the stud that connected to the load cell as the melt entered from sprue into the rod relatively fast, due to the sudden change in the cross sections, and hit the stud.

The load evolutions shown by these obtained experimental curves are generally similar, but some differences are found at the beginning. With the solidification proceeding, the load increases, reaches to a maximum and then decrease or becomes stable for a while and increases again. This force drop indicates the formation of the hot tearing in the casting. The temperature corresponding to the beginning of the force drop is considered as an initiation temperature of hot tear. The different alloys have different hot tearing initiation temperatures. For Mg-0.2 wt.% Y alloy, the hot crack initiated at 605.8 °C, which corresponds to a solid fraction of 0.997 (Fig.8 (a)). For Mg-0.9 wt.% Y alloy, the hot crack initiated at 598 °C at which the solid fraction is 0.989 (Fig.8 (b)). In addition, the force of Mg-0.9 wt.% Y alloy is dropping for a long time, it means the hot cracks are propagating larger than other alloys. Normally, the sharper and longer the force drop is, the larger the crack size is. Unlike aforementioned two alloys, the force curve of Mg-1.5 wt.% Y, does not show any force drop. However, the analysis of the castings (shown in the next section) indicates that hot tearing occurred in this alloy too. In this situation, according to Huang et al [30], the onset of hot tearing can be identified by locating the point at which the load as a function of time changes from linear increment to non-linear increment in the force curve. Hence the initiation temperature of hot tearing for Mg-1.5 wt.% Y alloy is found to be 616.6 °C . This temperature corresponds to a

solid fraction of 0.956, which is very close to the well established knowledge that hot tearing normally occurs at the latest stage of solidification when an approximate 5% liquid is left [1]. Similar way, the initiation temperature of hot tearing for Mg-4 wt.% Y can also be calculated using the above mentioned procedure, which shows that the corresponding solid fraction is 0.918.

4.2 Microstructural observations

4.2.1 As-cast

Fig.9 shows the optical micrographs of binary Mg-Y alloys taken near the junction of the sprue and the horizontal rod. From the microstructure, it can be seen that with increasing the content of Y the microstructure is changed from columnar grains to equiaxed grains. However, Mg-0.9 wt.% Y alloy exhibits columnar grain and largest grain size among all the alloys. Equiaxed grains are dominant in Mg-4 wt.% Y alloy.

4.2.2 Observations of hot cracks

Fig.10 shows the macro view of the cracks on the surfaces of the restrained rods for binary Mg-Y alloy castings. It can be seen that the compositions of alloys largely influenced the hot cracks. No macro-cracks are observed near the junctions of Mg-0.2 wt.% Y and Mg-4 wt.% Y alloys. In contrast, the macro-cracks are clearly observed near the junctions of Mg-0.9 wt.% Y and Mg-1.5 wt.% Y alloys. The large open crack in the former alloy casting than that of the latter, indicates that Mg-0.9 wt.% Y has the largest hot tearing tendency among all these four alloys.

Fig.11 shows the X-ray tomography photographs of the hot cracks located in the centre of rods (2D centre slice). Very few cracks are observed in Mg-0.2 wt.% Y and Mg-4 wt.% Y alloys. The alloy with 0.9 wt.% Y has a large volume of crack. In this sample, the initiation of hot cracks at the junctions can clearly be traced down towards the center of the rod. Compared with Mg-0.9 wt.% Y alloy, the amount of cracks decreased in Mg-1.5 wt.% Y alloy. In addition, in alloy with the content of 4 wt.% Y, few white river patterns are noticed. This indicates the presence of high X-ray observed materials in that region which is probably the high content of Y. It is noticed that these white river

patterns are normally observed near the main cracks. In addition, in all rods the most of hot cracks locate near the surface. In contrast, near the centre of rod the hot cracks are hardly found.

Fig.12 shows SEM micrographs of hot cracks on the longitudinal surfaces. It can be seen that all hot cracks propagate along the dendritic or grain boundaries. The main cracks normally initiates at sprue-rod junction. In front of these main cracks, phases with different contrast are observed. At high magnifications, it can be seen that they are second phases (Fig.12). EDS analysis indicates that these regions are Y rich (Fig.13). In Mg-4 wt.% Y alloys, the content of Y in the white region can reach to 32.43 wt.%. Another interesting phenomenon is that, with increasing the content of Y the amount of white river patterns increases. These river patterns can be seen clearly in Fig.13, which contains eutectic phases.

Fig.14 shows the fracture surfaces at the hot tear regions of Mg-0.9 wt.% Y and Mg-1.5 wt.% Y alloys. The morphology of the fracture surface showing the typical features of hot tearing, i.e. interdendritic and intergranular fractures. Normally the features of hot crack surfaces are smooth. Besides the smooth surfaces caused by the interdendritic separations, the transgranular fractures are also observed. These tearing fractures are caused by the subsequent propagation of hot cracks. Interestingly, in some areas, shown in Fig.14, a thin layer of material is observed on the fracture surface with a fluvial pattern. The EDS analysis result indicates that these layers are rich in Y content. This demonstrates that the hot tearing is an interdendritic separation, which happens when there still exists a liquid layers with solute segregation at the dendritic boundaries.

4.3 Quantitative measurement of crack volume

Fig.15 shows the total crack volume measured by X-ray micro-tomography technique. The total crack volume depends on the content of Y. It increases with the content of Y, reaches to a maximum at about 0.9 wt.% Y and then reduces with further increasing the content of Y. The maximum volume of hot cracks measured for Mg-0.9 wt.% Y is about 58.1 mm^3.

5 Discussion

5.1 Comparison of thermodynamic calculations with experimental results

From Fig.5 and Fig.15, it can be concluded that the thermodynamic calculation results are quite in agreement with that obtained by experimental tests. Both of them indicate that the hot tearing susceptibility changes with Y content and follows "λ" shape even though the used parameters to evaluate the hot tearing susceptibility in both cases are different. For thermodynamic calculations, the parameter (see Equation 1) proposed by Clyne and Davies was used to estimate the hot tearing susceptibility [22]. While in the experiments the parameter "crack volume" was directly used to evaluate the hot tearing susceptibility. Indeed, these two parameters have no direct relations. However, they are practically useful to evaluate how the composition of primary alloying element influences the hot tearing susceptibility of alloys. Especially for the parameter used in thermodynamic calculations, it would be quite useful during alloy design when the experimental measurements of hot tearing susceptibility become difficult. Based on the present results, it can be concluded that it is reasonable to use the Clyne and Davies model to evaluate the influence of compositions on the hot tearing susceptibility.

Although Fig.5 and Fig.15 show similar shapes of the hot tearing susceptibility curves and indicate almost the same peak susceptibility (at 1 to 1.5 wt.% Y), a discrepancy between them still exists (Fig.16), i.e. the shape of the curve after the peak susceptibility. The crack volume reduces sharply after the peak in the experimental work whereas CSC curve reduces gradually in the model. This discrepancy is caused by the limitations of Clyne and Davies model. In their model, the definition of vulnerable period during which the hot tearing is easy to occur is not defined so accurately. They defined this period ($0.9 < f_s < 0.99$) only based on the previous experimental results. In some case, the hot tearing may happen with a liquid fraction of more than 0.1 [10, 15, 22]. In addition, Clyne and Davies model used a fixed equation to estimate the cooling rate which was simplified based on the situation of heat flow [22]. They did not incorporate the influence of mold temperature in their equation. Even so, Clyne and Davies model is still useful to

have first hand information on the influence of the alloy compositions on the hot tearing of an alloy.

5.2 Influence of the Y content on hot tearing susceptibility

In the present investigations, the hot tearing susceptibility of Mg-Y alloys is influenced by the content of Y in two ways: solidification range and microstructure. Normally, the hot tearing susceptibility is proportional to the solidification range, especially the vulnerable solidification region from the solid fraction 0.9 to 0.99 [22], which can be defined as follows:

$$\Delta T = T_{0.9} - T_{0.99} \tag{2}$$

Where ΔT is the temperature difference between the temperature at a solid fraction of 0.9 ($T_{0.9}$) and 0.99 ($T_{0.99}$). The large value of ΔT can lead to increase the hot tearing susceptibility. Table 1 lists the ΔT values obtained by thermodynamics calculations. As shown in Table 1, the vulnerable solidification region depends on the composition of Mg-Y alloys. ΔT increases with the content of Y to 1.5 wt.%, and then decreases with further increasing the content of Y more than 4 wt.%. Both Mg-0.9 wt.% Y and Mg-1.5 wt.% Y alloys have a lager freezing range than other two alloys. The time spending in the vulnerable solidification zone is much longer, demonstrating that the possibility of hot cracking initiation is larger. This result is also in agreement with that obtained by experimental measurements, which shown that Mg-0.9 wt.% Y and Mg-1.5 wt.% Y alloys have more cracks.

The addition of Y in Mg affects the grain morphology, which is considered one of the most important factors to influence the initiation of hot tearing [31-32]. The grains with a large size and columnar structure promote easy initiation and propagation of hot crack. In contrast, a fine grain size and equiaxed structure helps to avoid the initiation of hot tearing. The fine microstructure is not only beneficial for accommodating the local deformation but also for the melt to flow due to the increased amount of grain boundaries. Hence the possibilities of refilling the fresh hot tears by the remaining liquid increases and as a consequence, these hot tears are possibly healed. As shown in Fig.9,

the grain size of Mg-0.9 wt.% Y alloy is the largest, and hence this alloy shows higher hot tearing susceptibility.

The amount of eutectic liquid is also regarded as one of the most important factors to influence the initiation of hot tearing [1-2], especially for binary alloys [33]. In Mg-Y alloys, the eutectic amount depends on the content of Y. Generally, the fluidity of melt increases with the amount of low melting point eutectic liquid. In the alloys with a high content of Y, the hot tearing susceptibility is low due to the large amount of eutectic liquid at the final stage of solidification which heals the cracks to a greater extent due to the high fluidity. Experimental results show that the hot tearing almost disappear when the content of Y is more than 4 wt.%. However, the second phases precipitated from the liquid above the solidus may act as nuclei for hot tearing initiation near the solidus. For the present investigated alloys, the influence of second phases on the hot tearing initiation may be neglected. The microstructure analyses confirm that second phases in these two alloys are very few (Fig.12 and Fig. 14). Also, for these two alloys, the solidification paths calculated using Scheil solidification model, indicate that the second phase fractions are almost near to zero (Fig.17). Even in Mg-4 wt.% Y alloy, only 2 mol% $Mg_{24}Y_5$ phase is expected to form.

5.3 Hot crack initiation, propagation and healing

As aforementioned, the hot tears initiate above the solidus temperature, i.e. at the final stage of solidification with small amount of liquid phase remained. With the solidification proceeding, the nucleation starts and the nucleus grow to become a dendrite. When the solid becomes dominant, the dendrites are interconnected. At these dendritic boundaries, the remained liquid film with a lower melting temperature possibly covers the surface of these dendrites. In the meantime, the thermal strain and stress could be formed during solidification. If they increase to a critical value, the interdendritic separation occurs. The formed thermal stress is then released. On the hot tearing curves, these drops in load can be observed. Fig.19 shows the onset temperature of hot tears and its corresponding solid fraction as a function of the content of Y. As shown, the solid fraction at which hot tearing initiates decreases with increasing the content of Y.

Recently, Gao et al. investigated the hot tearing behavior of Mg-Al-Sr alloys [7]. They also found that this critical solid fraction depends on the content of alloying element Al: with increase in Al content, it reduces.

Most of earlier investigations illustrated that the hot tearing is normally initiated at a remained solid fraction of about 0.95 (as aforementioned). However, with the improvement of theoretical modeling and experimental techniques, this value may vary even below 0.95 depending on the alloy and solidification conditions. The present results have confirmed that this value really depends on the content of Y (Fig.19). It changes from 0.916 to 0.997. In a recent review [2], Eskin summarized the related literature and indicated that this value is in the range from 0.85 to 0.95. Interestingly, Cao's investigations further showed that the hot tears can be initiated even at a lower remained solid fraction of 0.78 [7]. Due to the fact that the solidification is a complex process, it is very difficult to measure this value accurately. The initiation of hot tearing is affected by many factors: not only the materials properties but also the casting parameters. In addition, even if the exact onset temperature is determined, the solid fraction corresponding to this temperature can not be error free as it is normally calculated using thermodynamic calculations. This is because the used solidification models such as equilibrium model or Scheil's model to calculate the solid fraction are different from the real solidification situation.

After the initiation of hot tears, they propagate along the dendritic and grain boundaries with the assistance of thermal stress during solidification (Fig.12 and Fig.18). The thermal stress is further released, leading to the further drop in the load (Fig.8), which is clearly reflected on the hot tearing curves. As indicated by Fig.14, the propagation of hot cracks in Mg-0.9 wt.% Y alloy is easy and proceeds by the interdendritic separations. In the fracture surface, a bumpy surface covered with a smooth layer is observed, which is a typical trace of solidified remained liquid film. The similar situation is seen in Mg-1.5 wt.% Y alloy. In this alloy, the hot crack still mainly propagates through interdendritic separations. Compared with Mg-0.9 wt.% Y alloy, the difference is that the amount of tears of interconnected dendrites increases in Mg-1.5 wt.% Y (Fig.18). This means that in

this alloy the propagations of hot cracks are possibly blocked by the interconnected regions. This can also explain why this alloy has slightly lower hot tearing susceptibility than Mg-0.9 wt.% Y alloy.

As shown in Fig.11 and Fig.12, the refilling of hot cracks by the remained liquid can be traced. After the hot cracks occur, the regions near them have a negative pressure [10, 34]. The negative pressure, suck back the liquid, and refilling of hot cracks may occur. This liquid is enriched with Y content, and hence their density is much higher than the average density of the alloy. This Y enriched solidified liquid is seen with white contrast in SEM and tomography. Refilling of hot cracks can be observed in the present four investigated alloys including the low Y containing alloy, Mg-0.2 wt.% Y (Fig.12). According to the force curve of Mg-0.2 wt.% Y (Fig.8), hot tearing should have occurred as the curves show a drop in load. However, the macro-observations (Fig.10) and X-ray tomography results (Fig.11) exhibit no hot cracks in this alloy. This inconsistence can be related to the early explained phenomenon "subsequent healing of hot cracks". Indeed, SEM observations have confirmed the refilling and healing of hot cracks in Mg-0.2 wt.% Y alloy (Fig.11 (a)). It seems that the refilling and healing phenomena are easier in the alloys with high contents of Y (Fig.11 (d) and Fig.12 (d)). More white river-like patterns have been observed in Mg-4 wt.% Y alloy. In the alloys with high content of Y, the amount of low meting point eutectics are high. The remained liquid has a higher flow-ability. This is why the hot cracks occurred in these alloys have a higher possibility to be healed. Moreover, due to the easy refilling and healing of hot cracks, no apparent drop in load is found on the hot tearing curve of Mg-4 wt.% Y alloy.

6 Conclusions

The hot tearing susceptibility of binary Mg-Y system has been investigated by thermodynamic calculation and experimental methods. The conclusions are summarized as follow:

(1) Both the experimental measurements and thermodynamic calculations show the same tendency in the variation of hot tearing susceptibility with Y content. The hot tearing susceptibility as a function of Y content follows "λ" shape. The CSC first

increases with Y content, reaches the maximum at about 1~2 wt.% Y and then decreases with further increasing the Y content.

(2) When a hot crack is initiated, a drop in load increment is observed on hot tearing curves. Its corresponding onset temperature can then be determined.

(3) The hot cracks are initiated at a critical solid fraction from 0.9 to 0.99. It decreases with increasing the content of Y. The hot cracks propagate along the dendritic or grain boundaries through the interdendritic separation or tearing of interconnected dendrites.

(4) The initiations and propagations of hot cracks are influenced by alloy compositions, grain morphology and size, solidification range and amount of eutectic. The maximum hot tearing susceptibility is obtained in Mg-0.9 wt.% Y alloy which is due to its large grain size and wide solidification range and presence of small amount of eutectic.

(5) The hot cracks could be healed by the subsequent refilling of remained liquids, and the degree of refilling depends on the amount of liquid available at the final stage of solidification.

Acknowledgements

The authors would like to thank Mr. G. Meister for the technical support, and Mrs. Petra Fischer for SEM observations. Financial supports from CSC-Helmholtz scholarship for Wang′ s PhD study in HZG are gratefully acknowledged.

References

[1] J. Campbell. Castings. Oxford: Butterworth-Heinemann, 2003.

[2] D.G. Eskin, Suyitno, L. Katgerman. Mechanical properties in the semi-solid state and hot tearing of aluminium alloys. Prog. Mater. Sci. 2004; 49: 629-711.

[3] J. Guo, M. Samonds. Modeling of casting and solidification processing. ASM Handbook, vol. 22A, ASM International Materials Park, OH, 2010.

[4] A. Ankara, H.B. Ari. Determination of hot crack susceptibility in various kinds of steels. Mater Design. 1996; 17: 261-265.

[5] M. Li, H.W. Wang, Z.J. Wei, Z.J. Zhu. The effect of Y on the hot-tearing resistance of Al-5 wt.% Cu based alloy. Mater Design. 2010; 31: 2483-2487.

[6] G. Cao, S. Kou. Hot tearing of ternary Mg-Al-Ca alloy castings. Metall. Mater. Trans. A. 2006; 37: 3647-3663.

[7] G Cao, I Haygood, S Kou. Onset of Hot Tearing in Ternary Mg-Al-Sr Alloy Castings. Metall. Mater. Trans. A. 2010; 41: 2139-2150.

[8] N. Hort, H. Dieringa, H. Frank, K.U. Kainer. Hot tearing of magnesium alloys. T Indian I Metals. 2005; 58: 703-708.

[9] M. Pekguleryuz, P. Vermette. Developing castability index for magnesium diecasting alloys. Int. J. Cast Metal. Res. 2009; 22: 357-366.

[10] Z.S. Zhen, N. Hort, O. Utke, Y.D. Huang, N. Petri, K.U. Kainer. Investigations on hot tearing of Mg-Al binary alloys by using a new quantitative method. Magnesium Technol. 2009; 105-110.

[11] L. Bichler, C. Ravindran. New developments in assessing hot tearing in magnesium alloy castings. Mater Design. 2010; 31: 517-523.

[12] Y.S. Wang, B.D. Sun, Q.D. Wang, Y.P. Zhu, W.J. Ding. An understanding of the hot tearing mechanism in AZ91 magnesium alloy. Mater. Lett. 2002; 53: 35-39.

[13] Y.S. Wang, Q.D. Wang, C.J. Ma, W.J. Ding, Y.P. Zhu. Effects of Zn and RE additions on the solidification behavior of Mg-9Al magnesium alloy. Mat. Sci. Eng. A. 2003; 342: 178-182.

[14] L. Zhou, Y.D. Huang, P.L. Mao, K.U. Kainer, Z. Liu, N. Hort. Investigations on hot tearing of Mg-Zn-(Al) alloys. Magnesium Technology 2011, edited by W. H.

Sillekens, S. R. Agnew, N. R. Neelameggham and S. N. Mathaudhu, San Diego, California, USA, 2011; 125-130.

[15] L. Zhou, Y.D. Huang, P.L. Mao, K.U. Kainer, Z. Liu, N. Hort. Influence of composition on hot tearing in binary Mg–Zn alloys. Int. J. Cast Metal. Res. 2011; 24: 170-176.

[16] P. Gunde, A. Schiffl, P. J. Uggowitzer. Influence of yttrium additions on the hot tearing susceptibility of magnesium-zinc alloys. Mat. Sci. Eng. A. 2010; 527: 7074-7079.

[17] S. Sandlöbes, M. Friák, S. Zaefferer, A. Dick, S. Yi, D. Letzig, Z. Pei, L.-F. Zhu, J. Neugebauer, D. Raabe. The relation between ductility and stacking fault energies in Mg and Mg-Y alloys. Acta Mater. 2012; 60: 3011-3021.

[18] B.L. Wu, Y.H. Zhao, X.H. Du, Y.D. Zhang, F. Wagner, C. Esling. Ductility enhancement of extruded magnesium via yttrium addition. Mat. Sci. Eng. A. 2010; 527: 4334-4340.

[19] Q.M. Peng, J. Meng, Y. Li, Y.D. Huang, N. Hort. Effect of yttrium addition on lattice parameter, Young's modulus and vacancy of magnesium. Mat. Sci. Eng. A. 2011; 528: 2106-2109.

[20] X. Zhang, K. Zhang, X. Deng, H.W. Li, Y.J. Li, M.L. Ma, N. Li, Y.L. Wang. Corrosion behavior of Mg–Y alloy in NaCl aqueous solution. Prog. Nat. Sci.: Mater. Int. 2012; 22: 169-174.

[21] T.W. Clyne, G.J. Davies. Comparision between Experimental Data and Theoretical Predictions Relating to Dependence of Solidification Cracking on Composition. Solidification and casting of metals, edited by Sheffield, UK. 1977; 275-278.

[22] T.W. Clyne, G.J. Davies. The Influence of composition on solidification cracking in binary alloy systems. Brit. Foundryman 1981; 74: 65-73.

[23] A.A. Nayeb-Hashemi, J.B. Phase Diagram of Binary Magnesium Alloys. Clark, Metal Park, OH: ASM International, 1988; 43-46.

[24] H.D. Zhao, G.W. Qin, Y.P. Ren, W.L. Pei, D. Chen, Y. Guo. The maximum solubility of Y in .ALPHA.-Mg and composition ranges of $Mg_{24}Y_5$-x and Mg_2Y_{1-x} intermetallic phases in Mg-Y binary system. J. Alloy Compd. 2011; 509: 627-631.

[25] PanEngine 7 User's Guide, CompuTherm LLC, 2000-2007.

[26] J.M. Drezet, M. Rappaz. Study of hot tearing in aluminum alloys using the ring mold test. Modeling of Casting, Welding and Advanced Solidification Processes VIII. San Diego, USA, TMS. 1998; 883-890.

[27] D. Warrington, D.G. McCartney. Development of a new hot-cracking test for aluminum alloys. Cast Metals. 1989; (2): 134-143.

[28] I.G. Watson, P.D. Lee, R. J. Dashwood, P. Simulation of the Mechanical properties of an Aluminum matrix composite using X-ray microtomography. Metall. Mater. Trans. A. 2006; 37: 551-558.

[29] J. Alkemper, P.W. Voorhees. Three-dimensional characterization of dendritic microstructures. Acta Mater. 2001; 49: 897-902.

[30] Y.D. Huang, Z. Wang, A. Srinivasan, K.U. Kainer, N. Hort. Metallurgical characterization of hot tearing curves recorded during solicitation of magnesium alloys. Acta Phys. Pol. A. 2012; 122: 497-500.

[31] A.K. Dahle, L. Arnberg. The rheological properties of solidifying aluminium foundry alloys. JOM 1996; 48: 34-37.

[32] M. Easton, J. Grandfield, D. StJohn, B. Rinderer. The Effect of grain refinement and cooling rate on the hot tearing of wrought aluminum alloys. Mater. Sci. Forum. 2006; 30: 1675-1680.

[33] S. Lin, C. Aliravci, M.O. Pekguleryuz. Hot-tear susceptibility of aluminum wrought alloys and the effect of grain refining. Metall. Mater. Trans. A. 2007; 38: 1056-1068.

[34] I. Farup, J.M. Drezet, M. Rappaz. In situ observation of hot tearing formation in succinonitrile-acetone. Acta Mater. 2001; 49: 1261-1269.

Figure captions

Fig. 1. Schematic diagram of liquid fraction vs. fraction time showing the calculation of CSC.

Fig. 2 Solid fraction vs. temperature for the binary Mg-Y alloys calculated using non-equilibrium (Scheil) modeling.

Fig. 3 Partition coefficient of Y and liquidus slope in Mg-Y binary system.

Fig. 4 Calculated cooling curves for Mg-1.5 wt.% Y alloy under three different cooling conditions.

Fig. 5 Calculated CSC value as a function of the content of Y.

Fig. 6 Schematic diagram of experimental setup, (a) complete setup, (b) CRC apparatus with sensor, (c) position of thermocouple for obtaining the temperature at which the hot crack is initiated.

Fig. 7 Photograph showing the machined sample used for X-ray tomography study.

Fig. 8 Typical curves of contraction force as a function of solidification time at a mold temperature of 250 °C: (a) Mg-0.2 wt.% Y, (b) Mg-0.9 wt.% Y, (c) Mg-1.5 wt.% Y, (d) Mg-4 wt.% Y.

Fig. 9 Optical microstructures of binary Mg-Y alloys showing the grain structure: (a) Mg-0.2 wt.% Y, (b) Mg-0.9 wt.% Y, (c) Mg-1.5 wt.% Y, (d) Mg-4 wt.% Y.

Fig. 10 Macro view of the cracks on the surfaces of the restrained rods of binary Mg-Y alloys: (a) Mg-0.2 wt.% Y, (b) Mg-0.9 wt.% Y, (c) Mg-1.5 wt.% Y, (d) Mg-4 wt.% Y.

Fig. 11 X-ray photographs of Mg-Y alloys showing crack morphologies: (a) Mg-0.2 wt.% Y, (b) Mg-0.9 wt.% Y, (c) Mg-1.5 wt.% Y, (d) Mg-4 wt.% Y.

Fig. 12 SEM micrographs showing the cracks near the sprue-rod junction: (a) Mg-0.2 wt.% Y, (b) Mg-0.9 wt.% Y, (c) Mg-1.5 wt.% Y, (d) Mg-4 wt.% Y.

Fig. 13 As-cast structure Mg-4 wt.% Y alloy. Also shown here the EDS results of point A: (a) SEM image, (b) magnified view of second phase, (c) EDS of point A.

Fig. 14 SEM micrographs of hot tear surfaces of (a) Mg-0.9 wt.% Y and (b) Mg-1.5 wt.% Y alloys.

Fig. 15 Total crack volume measured by X-ray micro-tomography for Mg-Y alloys.

Fig. 16 Comparison of predicted CSC and experimental hot tearing tendency for Mg-Y binary alloys.

Fig. 17 Solidification processes of (a) Mg-0.9 wt.% Y and (b) Mg-4 wt.% Y, which are calculated using Scheil's model.

Fig. 18 Bridging of hot cracks at 250 °C mold temperature: (a) Mg-0.9 wt.% Y, (b) Mg-1.5 wt.% Y.

Fig. 19 Initiation temperature of hot tearing and its corresponding solid fraction as a function of the Y content.

Table caption

Table 1 Hot tearing features and predicted vulnerable temperature ranges of Mg-Y alloys.

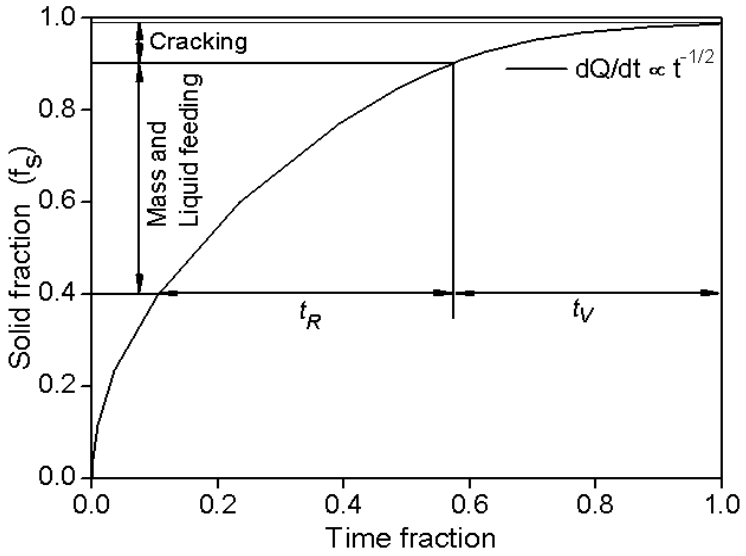

Fig. 1. Schematic diagram of liquid fraction vs. fraction time showing the calculation of CSC.

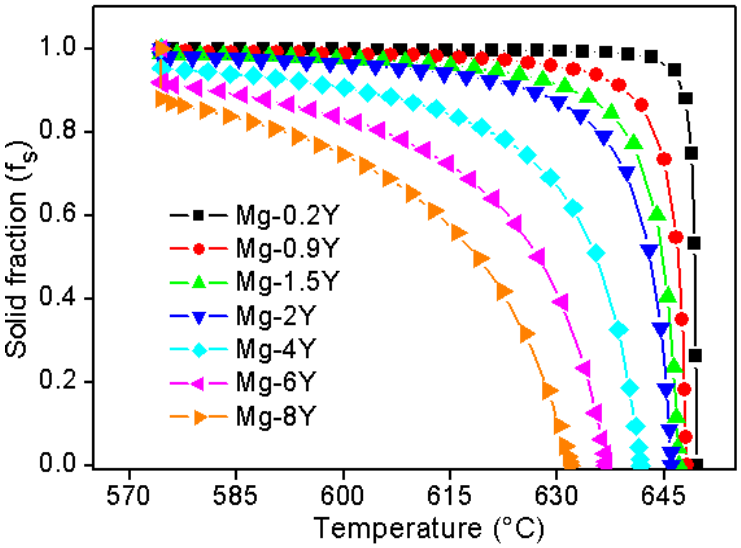

Fig. 2 Solid fraction vs. temperature for the binary Mg-Y alloys calculated using non-equilibrium (Scheil) modeling.

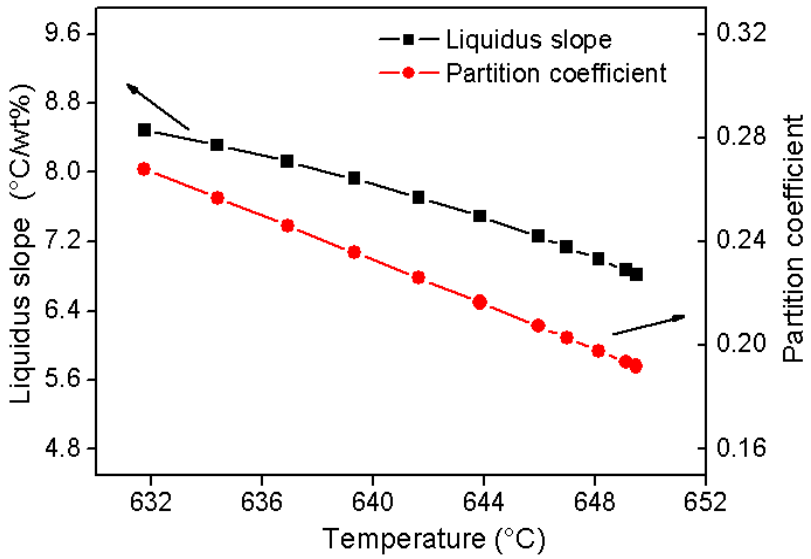

Fig. 3 Partition coefficient of Y and liquidus slope in Mg-Y binary system.

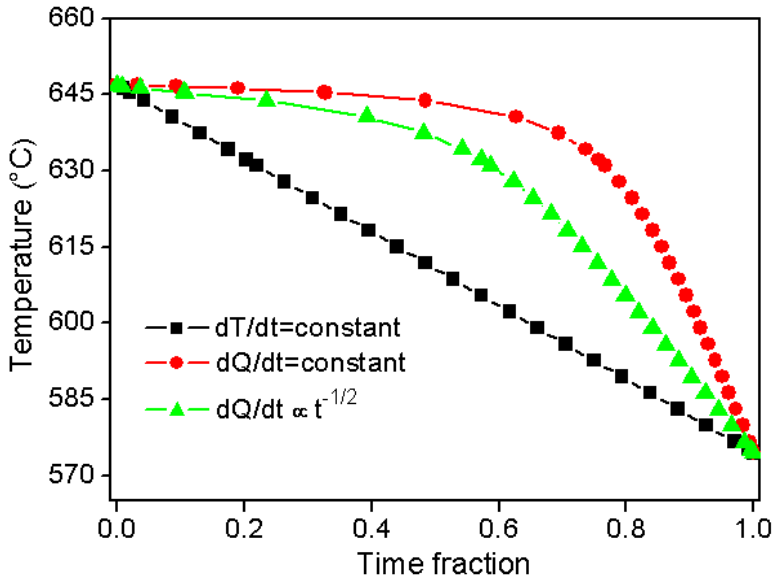

Fig. 4 Calculated cooling curves for Mg-1.5 wt.% Y alloy under three different cooling conditions.

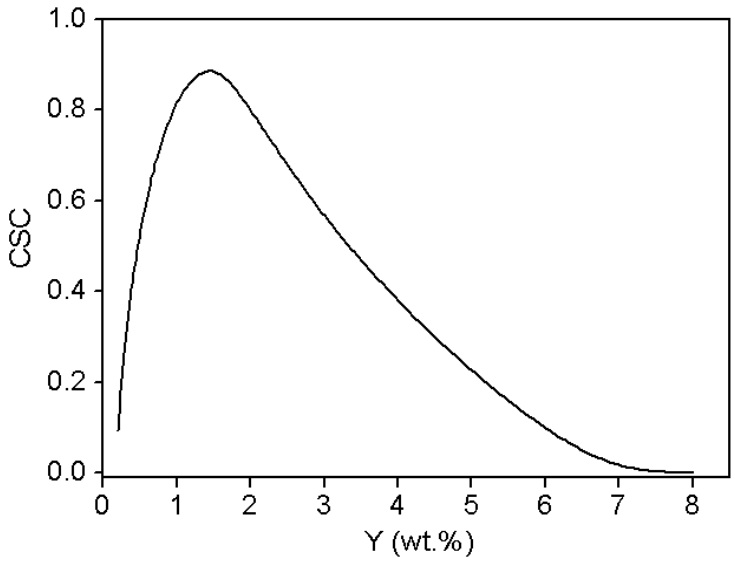

Fig. 5 Calculated CSC value as a function of the content of Y.

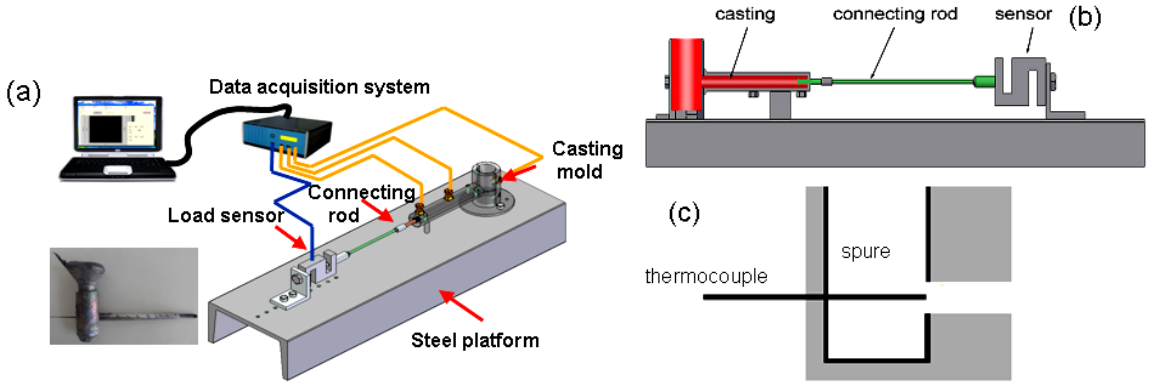

Fig. 6 Schematic diagram of experimental setup, (a) complete setup, (b) CRC apparatus with sensor, (c) position of thermocouple for obtaining the temperature at which the hot crack is initiated.

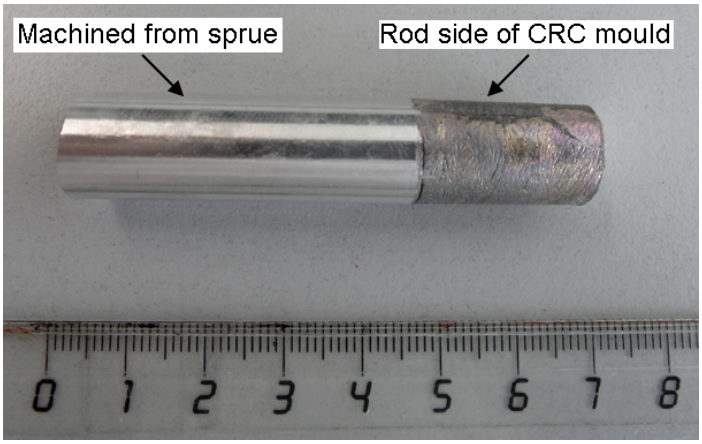

Fig. 7 Photograph showing the machined sample used for X-ray tomography study.

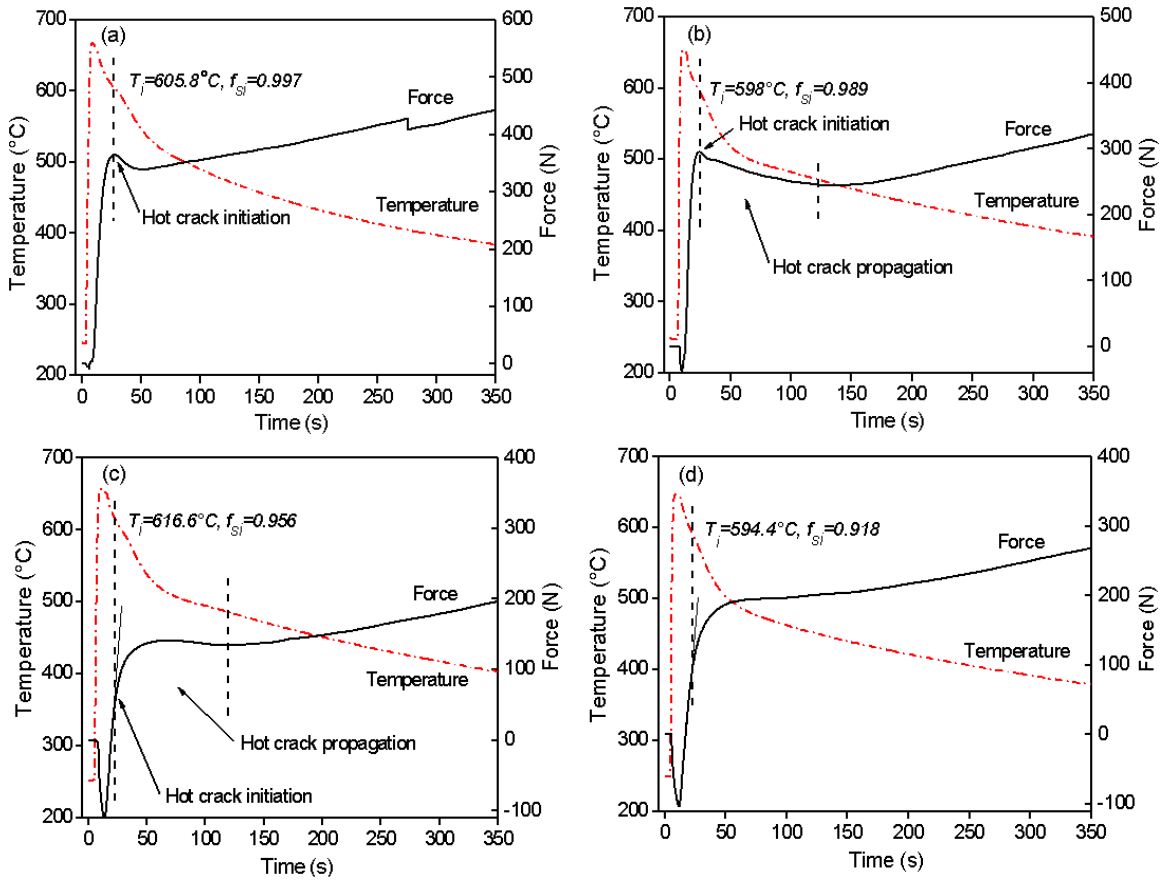

Fig. 8 Typical curves of contraction force as a function of solidification time at a mold temperature of 250°C: (a) Mg-0.2 wt.% Y, (b) Mg-0.9 wt.% Y, (c) Mg-1.5 wt.% Y, (d) Mg-4 wt.% Y.

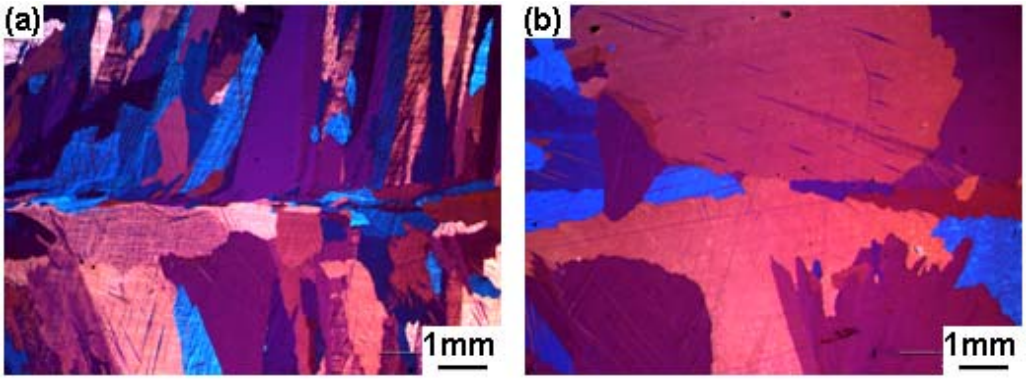

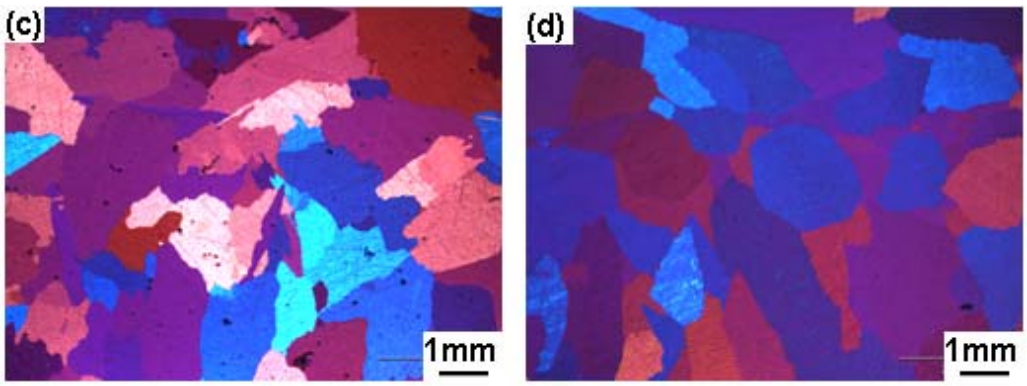

Fig. 9 Optical microstructures of binary Mg-Y alloys showing the grain structure: (a) Mg-0.2 wt.% Y, (b) Mg-0.9 wt.% Y, (c) Mg-1.5 wt.% Y, (d) Mg-4 wt.% Y.

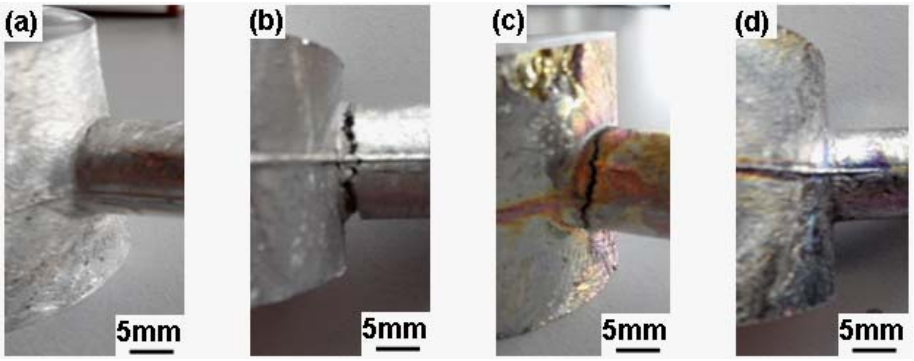

Fig. 10 Macro view of the cracks on the surfaces of the restrained rods of binary Mg-Y alloys: (a) Mg-0.2 wt.% Y, (b) Mg-0.9 wt.% Y, (c) Mg-1.5 wt.% Y, (d) Mg-4 wt.% Y.

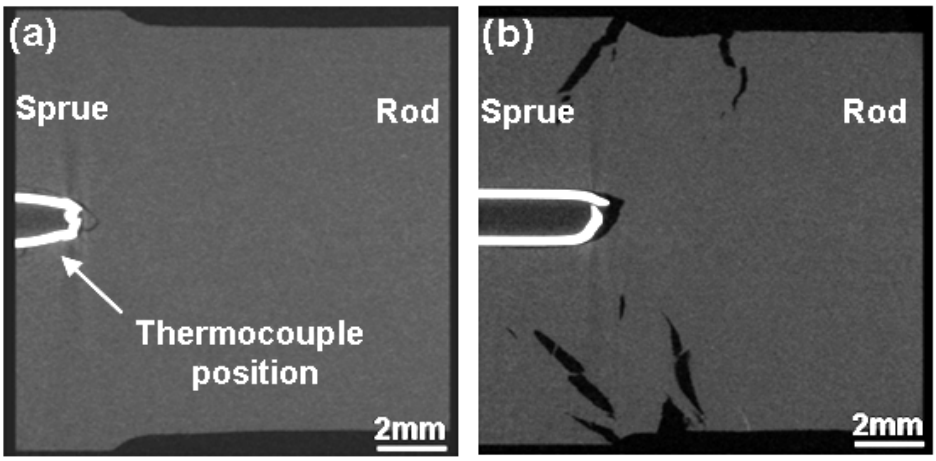

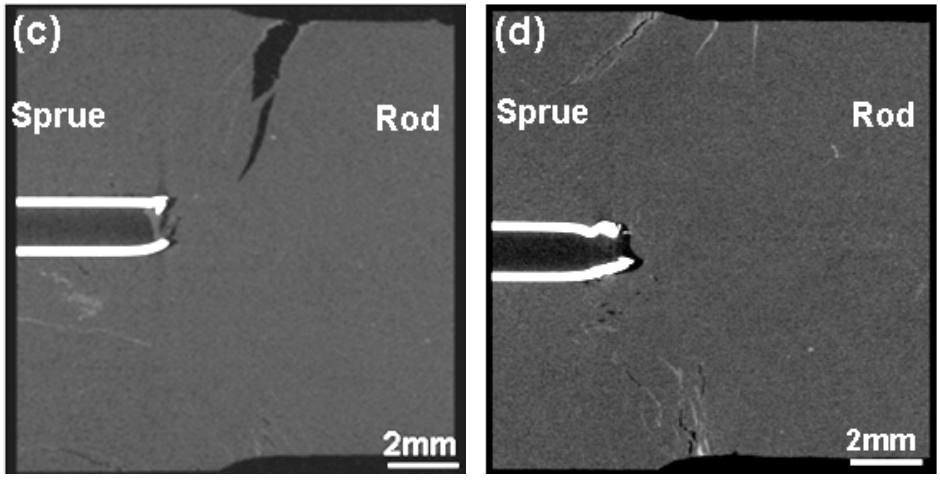

Fig. 11 X-ray photographs of Mg-Y alloys showing crack morphologies: (a) Mg-0.2 wt.% Y, (b) Mg-0.9 wt.% Y, (c) Mg-1.5 wt.% Y, (d) Mg-4 wt.% Y.

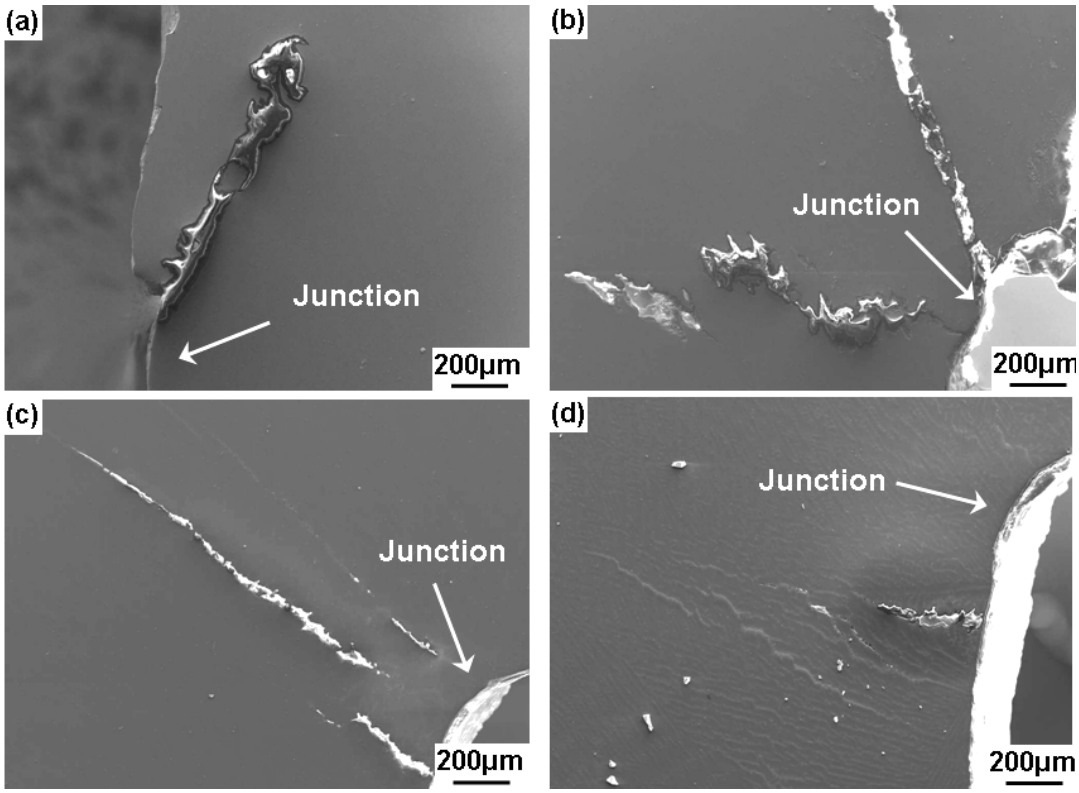

Fig. 12 SEM micrographs showing the cracks near the sprue-rod junction: (a) Mg-0.2 wt.% Y, (b) Mg-0.9 wt.% Y, (c) Mg-1.5 wt.% Y, (d) Mg-4 wt.% Y.

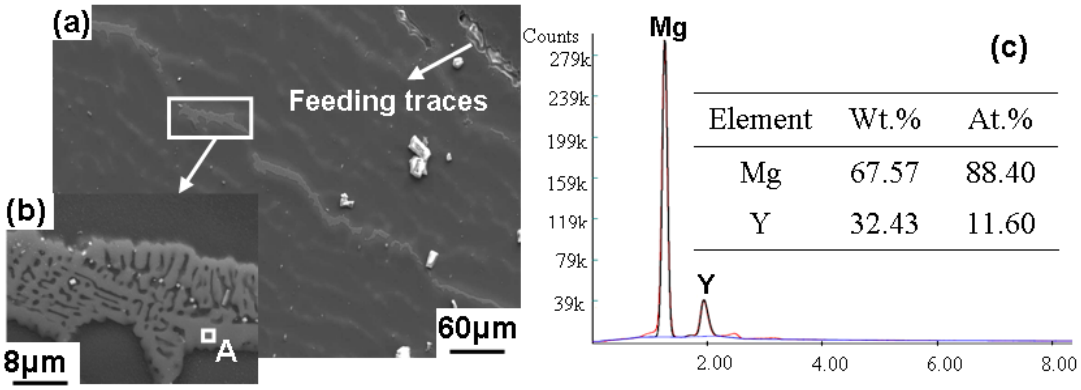

Fig. 13 As-cast structure Mg-4 wt.% Y alloy. Also shown here the EDS results of point A: (a) SEM image, (b) magnified view of second phase, (c) EDS of point A.

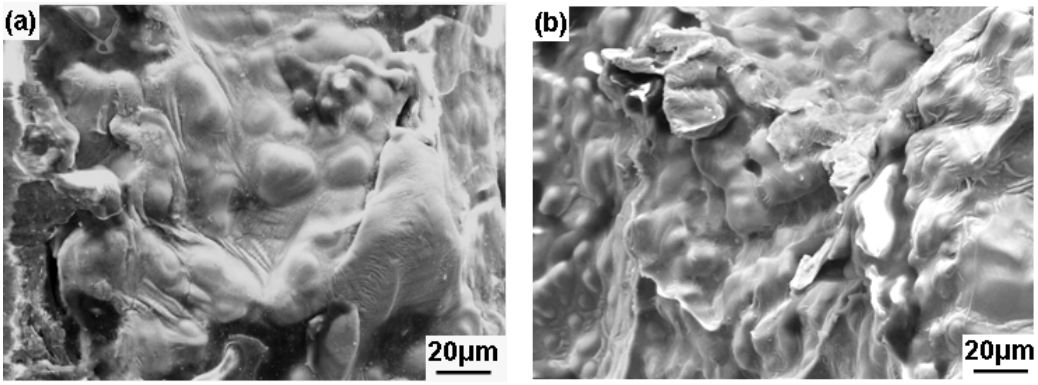

Fig. 14 SEM micrographs of hot tear surfaces of (a) Mg-0.9 wt.% Y and (b) Mg-1.5 wt.% Y alloys.

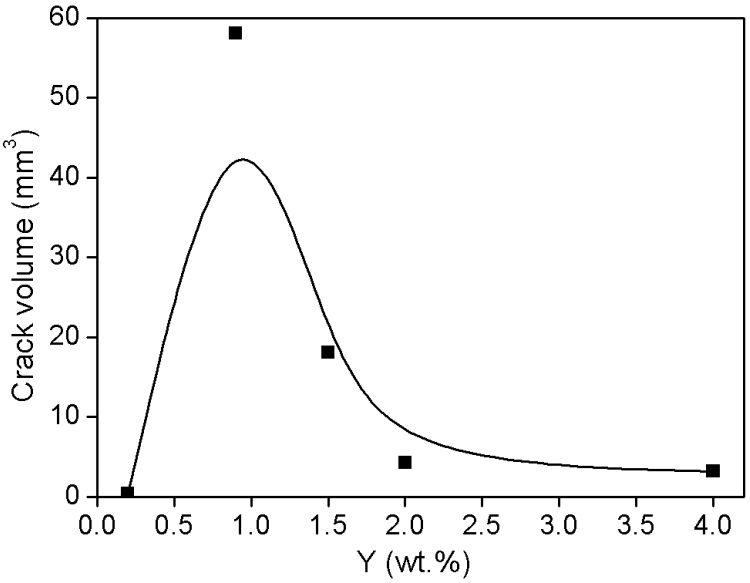

Fig. 15 Total crack volume measured by X-ray micro-tomography for Mg-Y alloys.

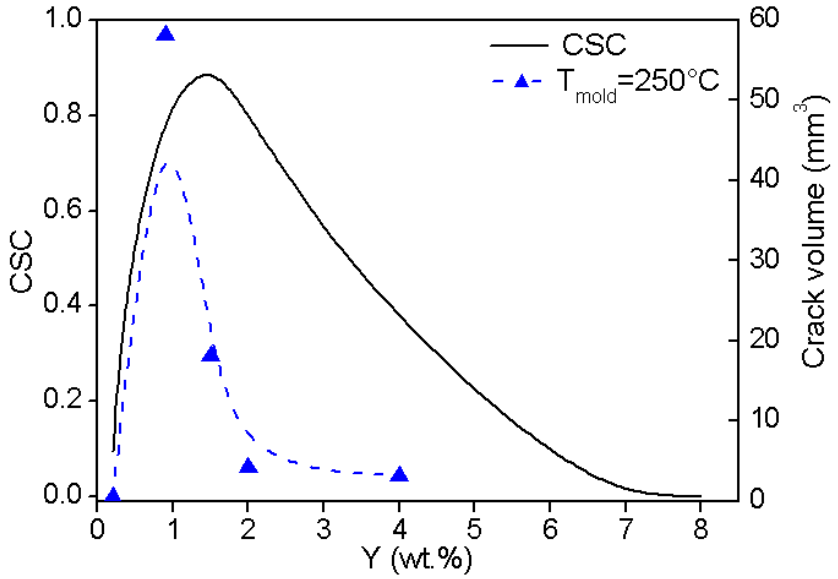

Fig. 16 Comparison of predicted CSC and experimental hot tearing tendency for Mg-Y binary alloys.

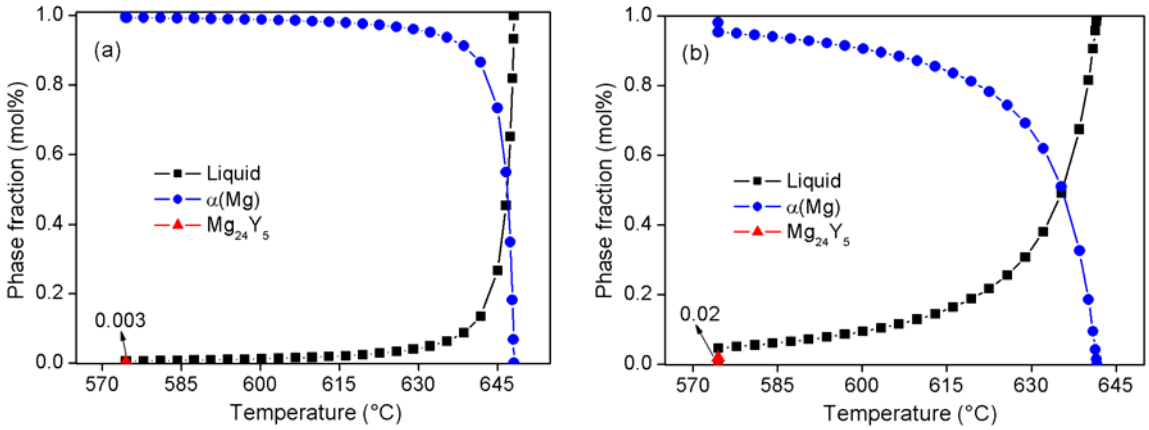

Fig. 17 Solidification processes of (a) Mg-0.9 wt.% Y and (b) Mg-4 wt.% Y, which are calculated using Scheil's model.

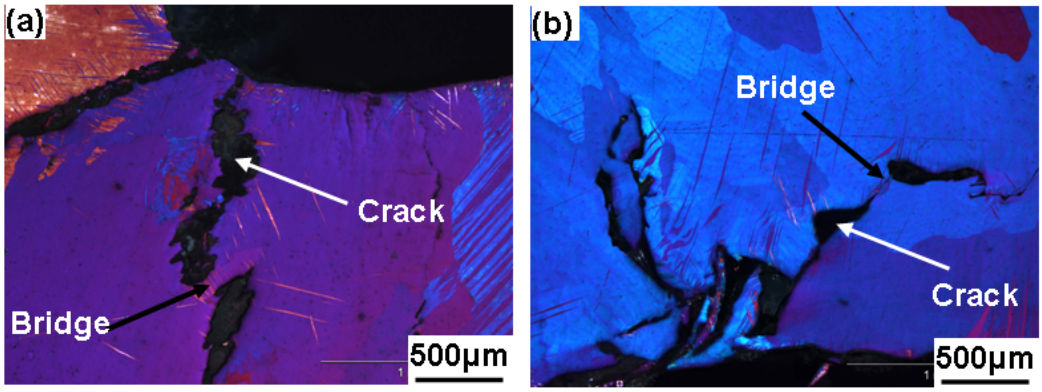

Fig. 18 Bridging of hot cracks at 250°C mold temperature: (a) Mg-0.9 wt.% Y, (b) Mg-1.5 wt.% Y.

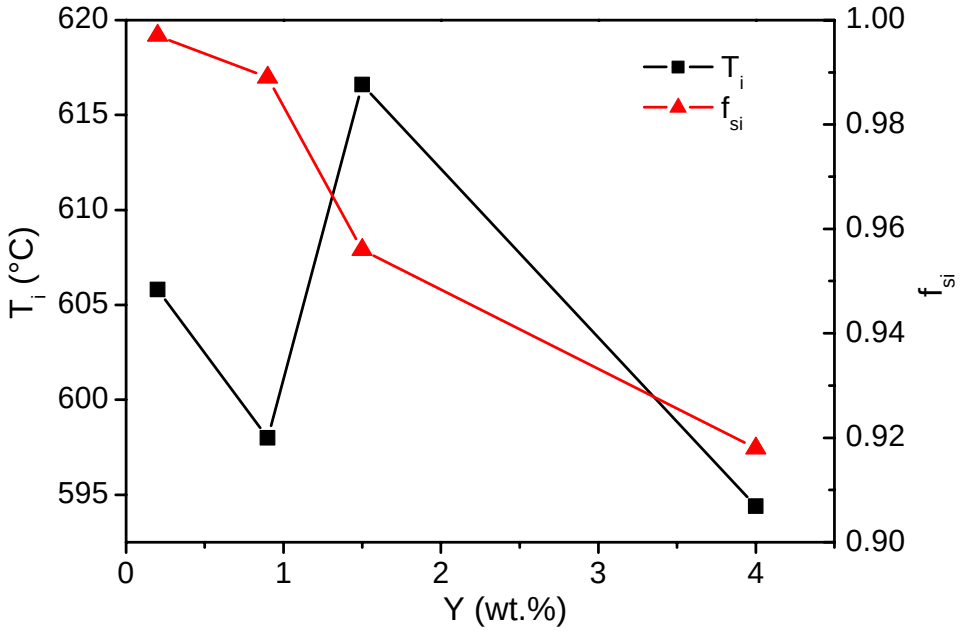

Fig. 19 Initiation temperature of hot tearing and its corresponding solid fraction as a function of the Y content.

Table 1 Hot tearing features and predicted vulnerable temperature ranges of Mg-Y alloys.

Alloy	$T_{0.9}$(°C)	$T_{0.99}$(°C)	ΔT(°C)
Mg-0.2 wt.% Y	644.39	637.89	6.50
Mg-0.9 wt.% Y	639.50	593.76	45.74
Mg-1.5 wt.% Y	632.21	574.45	57.76
Mg-4 wt.% Y	601.93	574.45	27.48